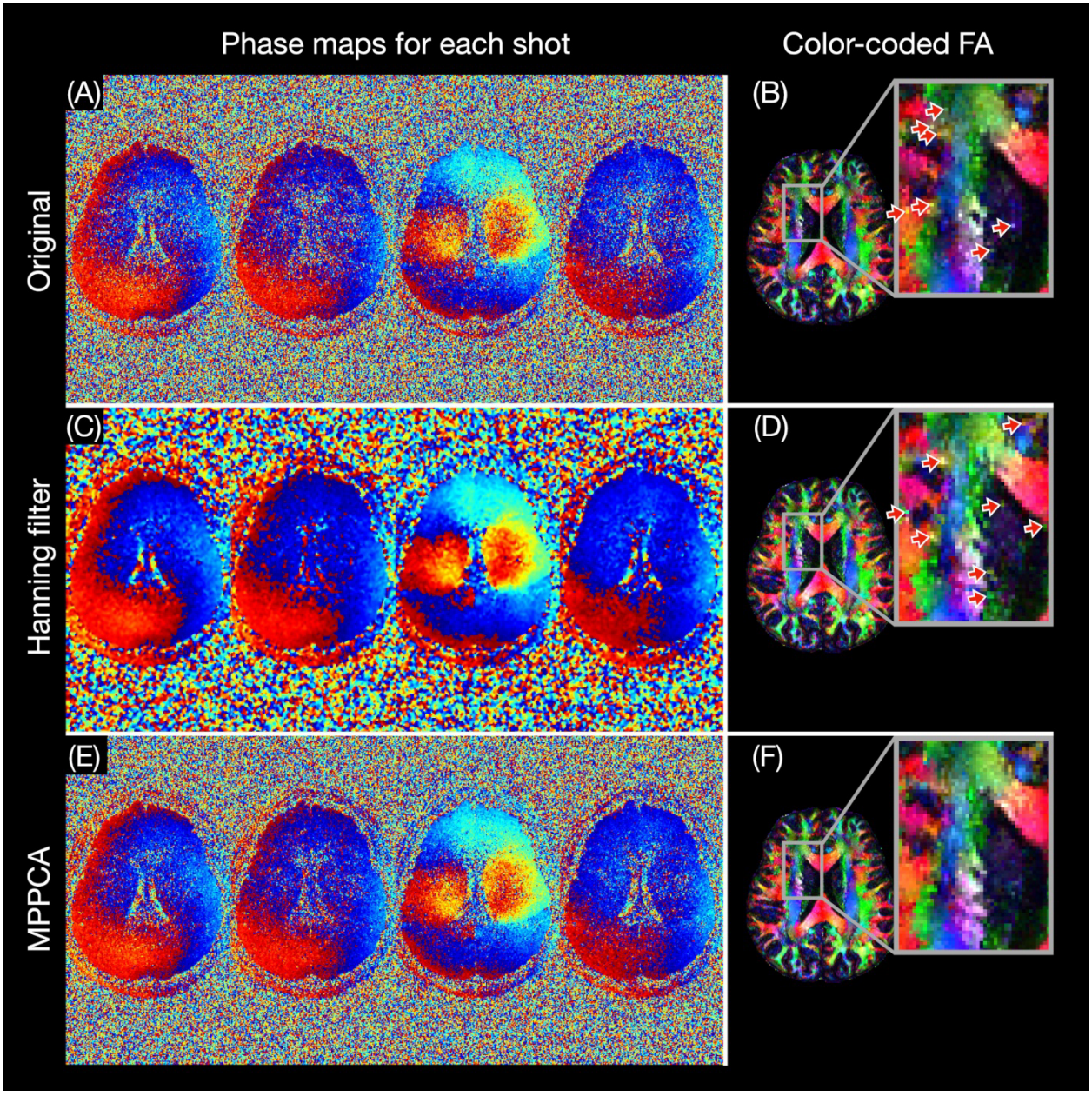

Supplementary Figure S1: Phase maps for each shot (**A**,**C**,**E**) and color-coded FA maps (**B**,**D**,**F**) from subject 3 with no smoothing or denoising of the phase maps (**A**,**B**), with a conventional smoothing of the phase maps using a Hanning filter (**C**,**D**), and with MPPCA denoising of the phase maps (**E**,**F**) in the MB-MUSE reconstruction. The arrows highlight areas with more noise in the FA maps.

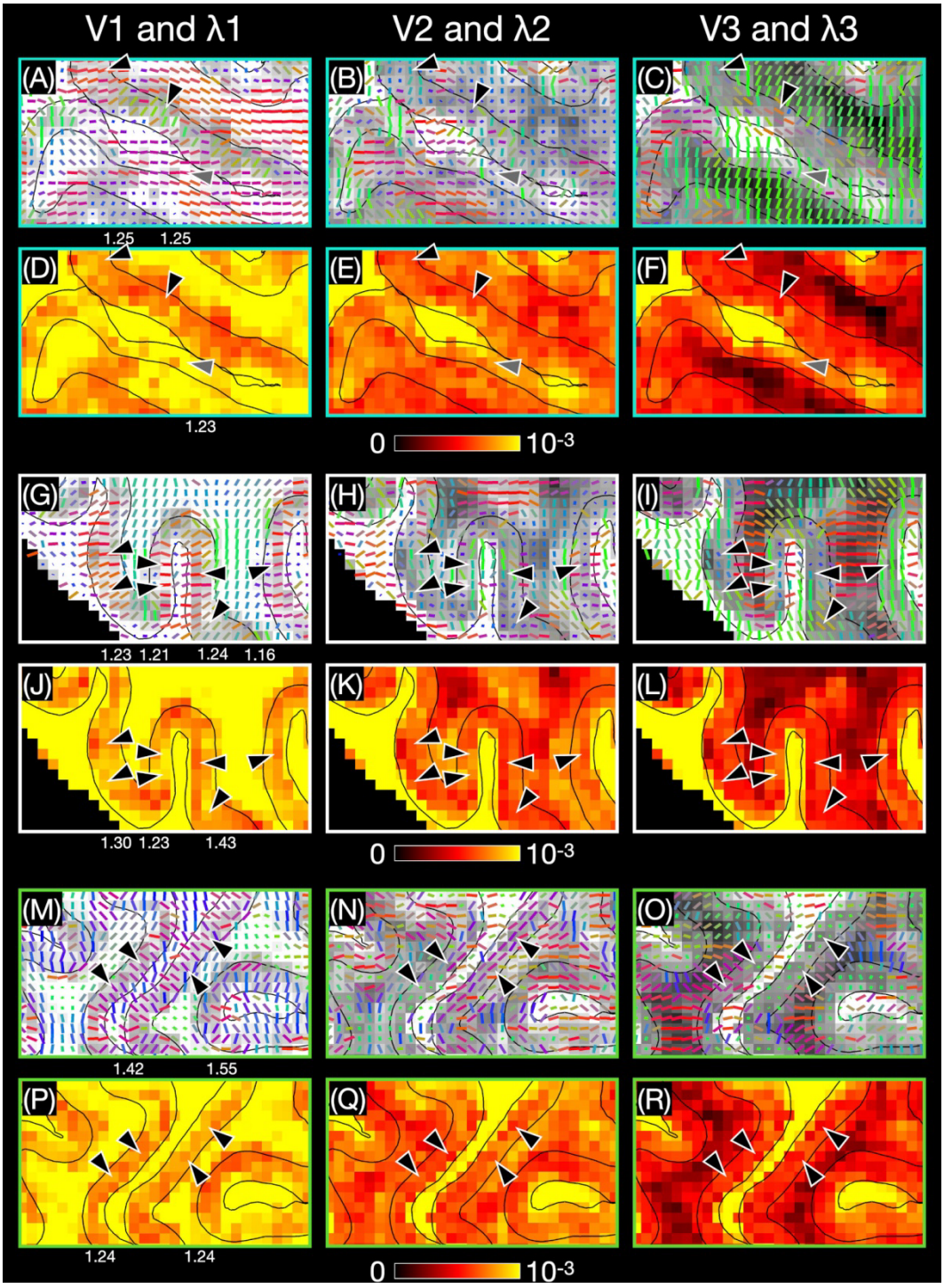

Supplementary Figure S2: Maps of the eigenvectors V1, V2, V3 (**A**–**C**, **G**–**I**, **M**–**O**) and eigenvalues λ_1, λ_2, λ_3 (**D**–**F**, **J**–**L**, **P**–**R**) in the same regions as those shown in Fig. 3.

The black arrowheads point to cortical regions with a primarily radial diffusion orientation and the gray arrowhead points to the primary somatosentory cortex in the postcentral gyrus with a primarily tangential diffusion orientation. The black lines denote the pial surface and WM/GM interface derived from the registered T_1-weighted anatomical images. The ratio between the first two eigenvalues λ_1/λ_2 is shown above and below the λ_1 maps for the representative voxels highlighted by arrowheads.

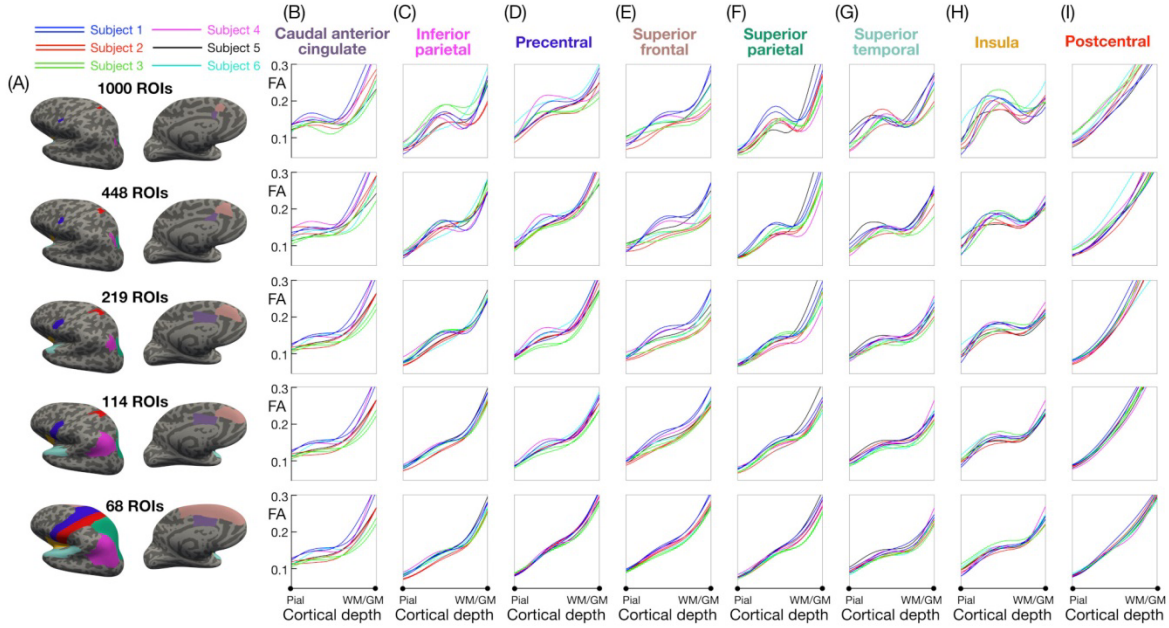

Supplementary Figure S3: (**A**) 8 representative ROIs from each of the 5 atlases. (**B-I**) FA vs. cortical depth profiles in each of these ROIs for both DTI scans from subjects 1-3 and the single DTI scan from subjects 4-6.

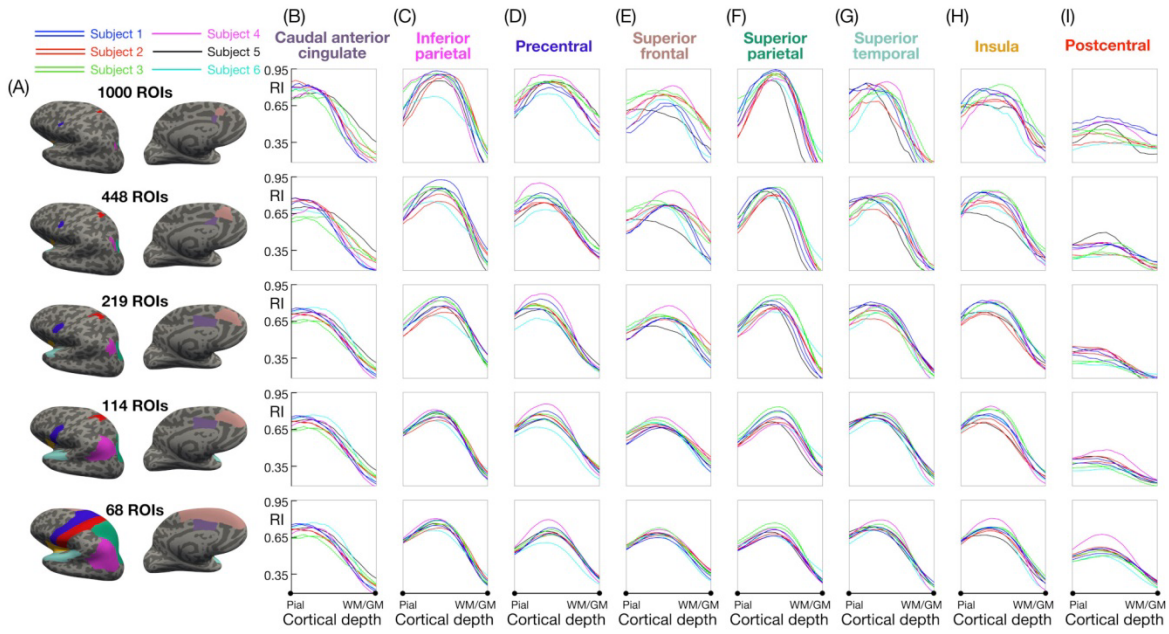

Supplementary Figure S4: (**A**) 8 representative ROIs from each of the 5 atlases. (**B-I**) RI vs. cortical depth profiles in each of these ROIs for both DTI scans from subjects 1-3 and the single DTI scan from subjects 4-6.

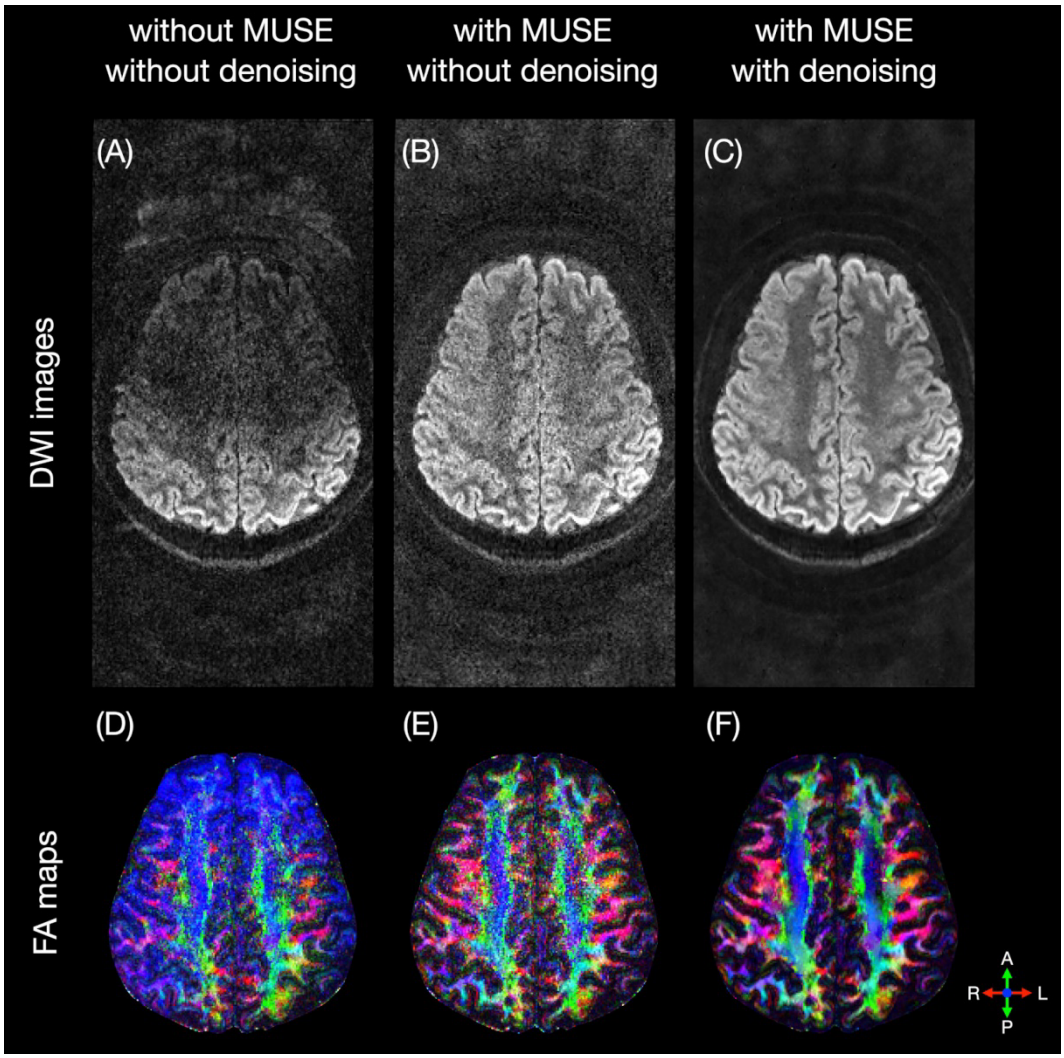

Supplementary Figure S5: DWI images (**A**–**C**) and color-coded FA maps (**D**–**F**) from subject 3 obtained without vs. with MUSE correction of motion-induced phase errors and without vs. with MPPCA denoising of the DWI images.

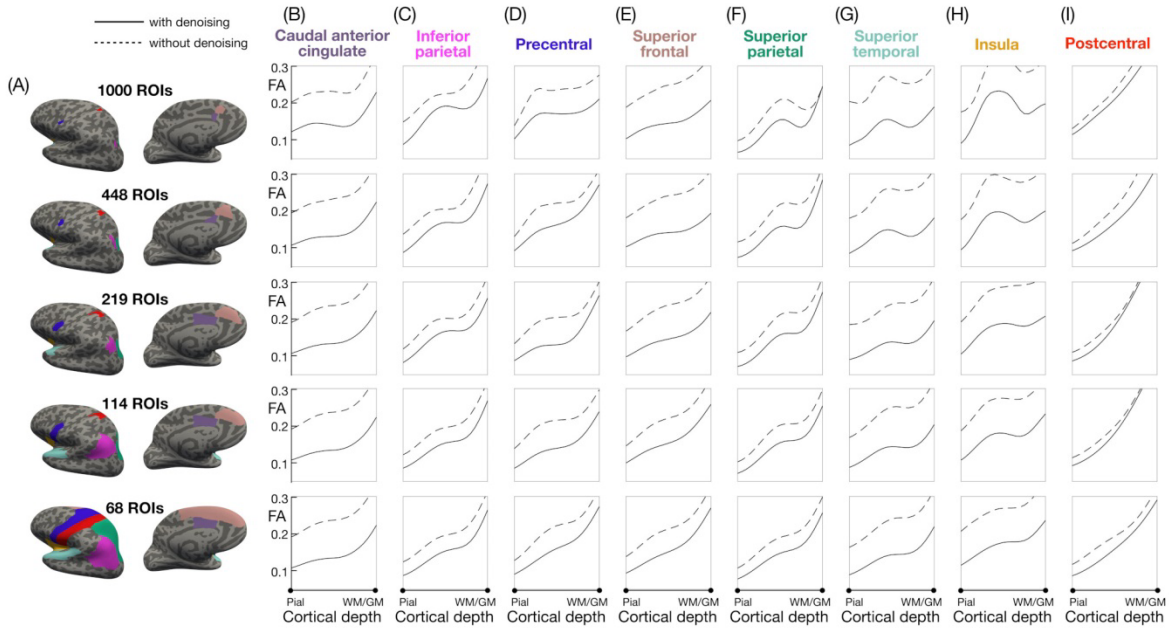

Supplementary Figure S6: (**A**) 8 representative ROIs from each of the 5 atlases. (**B-I**) FA vs. cortical depth profiles in each of these ROIs from subject 3 without (dashed lines) vs. with (solid lines) MPPCA denoising of the DWI images (and with all other parameters in the data analysis pipeline as used in Fig. 4).

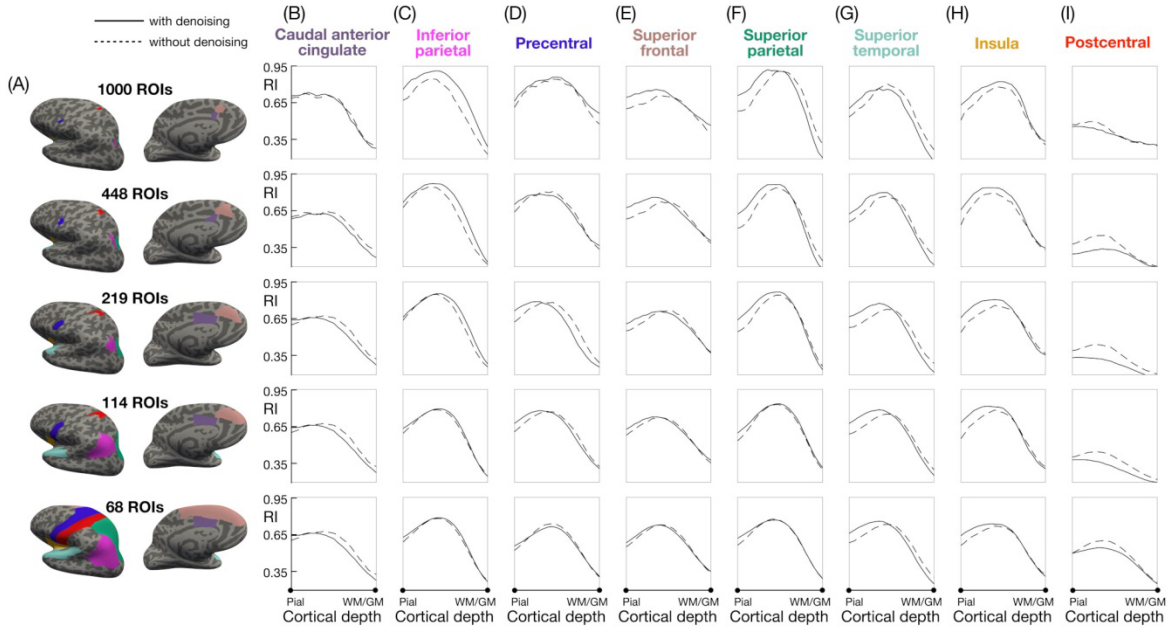

Supplementary Figure S7: (**A**) 8 representative ROIs from each of the 5 atlases. (**B-I**) RI vs. cortical depth profiles in each of these ROIs from subject 3 without (dashed lines) vs. with (solid lines) MPPCA denoising of the DWI images (and with all other parameters in the data analysis pipeline as used in Fig. 4).

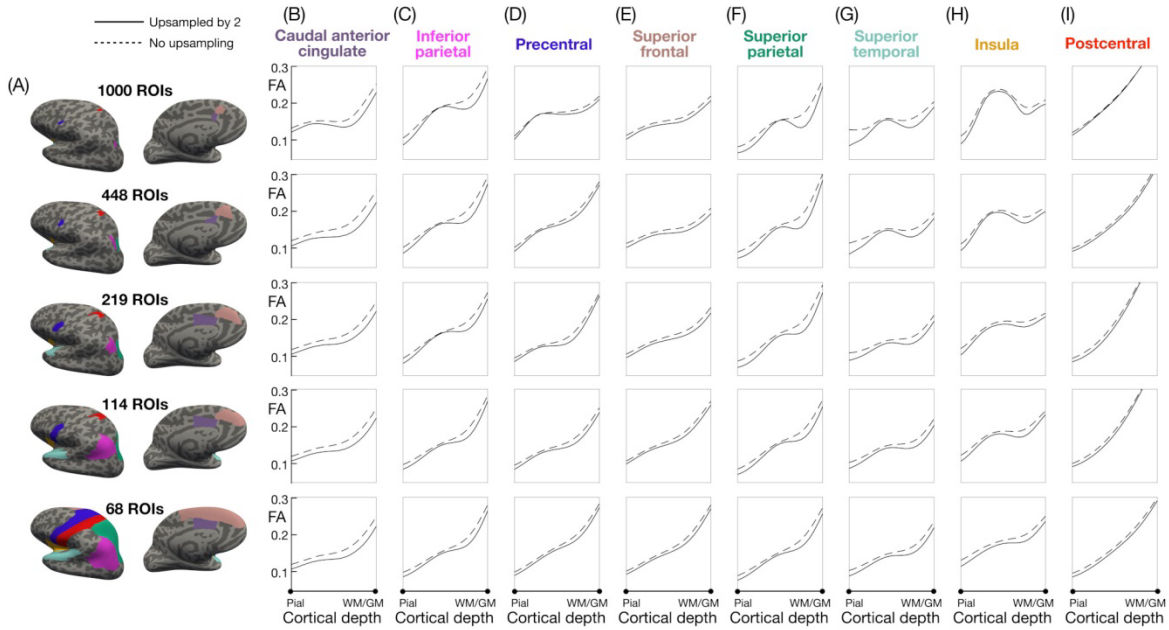

Supplementary Figure S8: (**A**) 8 representative ROIs from each of the 5 atlases. (**B-I**) FA vs. cortical depth profiles in each of these ROIs from subject 3 obtained without (dashed lines) vs. with (solid lines) upsampling the DWI images by a factor 2 before calculating the diffusion tensor (and with all other parameters in the data analysis pipeline as used in Fig. 4).

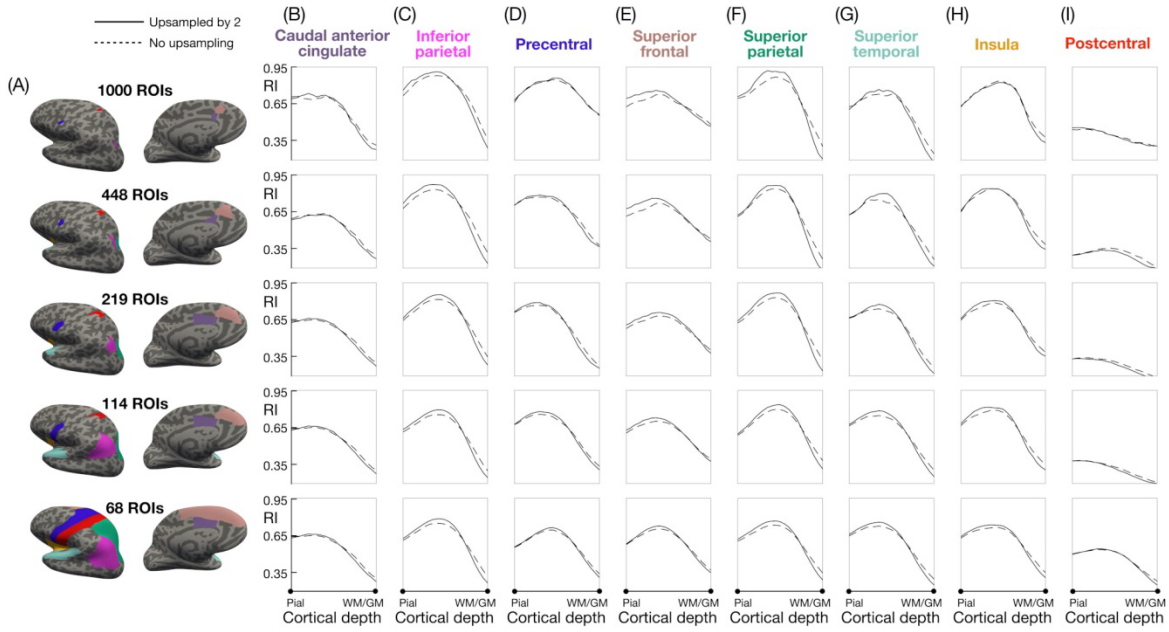

Supplementary Figure S9: (**A**) 8 representative ROIs from each of the 5 atlases. (**B-I**) RI vs. cortical depth profiles in each of these ROIs from subject 3 obtained without (dashed lines) vs. with (solid lines) upsampling the DWI images by a factor 2 before calculating the diffusion tensor (and with all other parameters in the data analysis pipeline as used in Fig. 4).

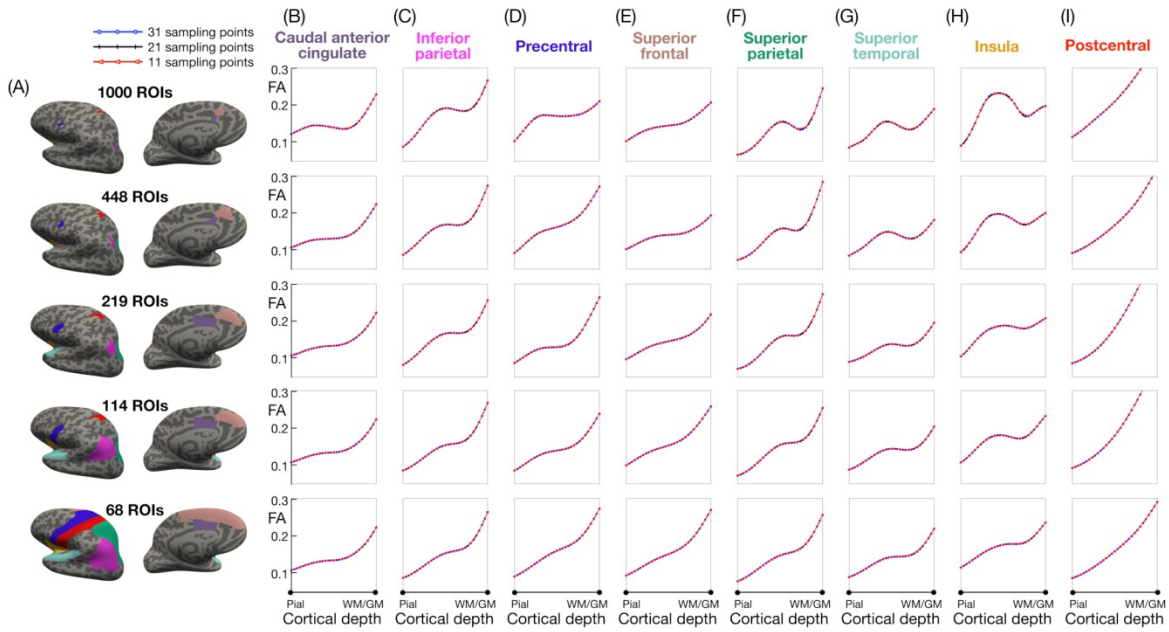

Supplementary Figure S10: (**A**) 8 representative ROIs from each of the 5 atlases. (**B-I**) FA vs. cortical depth profiles in each of these ROIs from subject 3 obtained with 11, 21, or 31 sampling points (i.e., with a step size of 10%, 5%, and 3.33% of the cortical thickness, respectively) (and with all other parameters in the data analysis pipeline as used in Fig. 4).

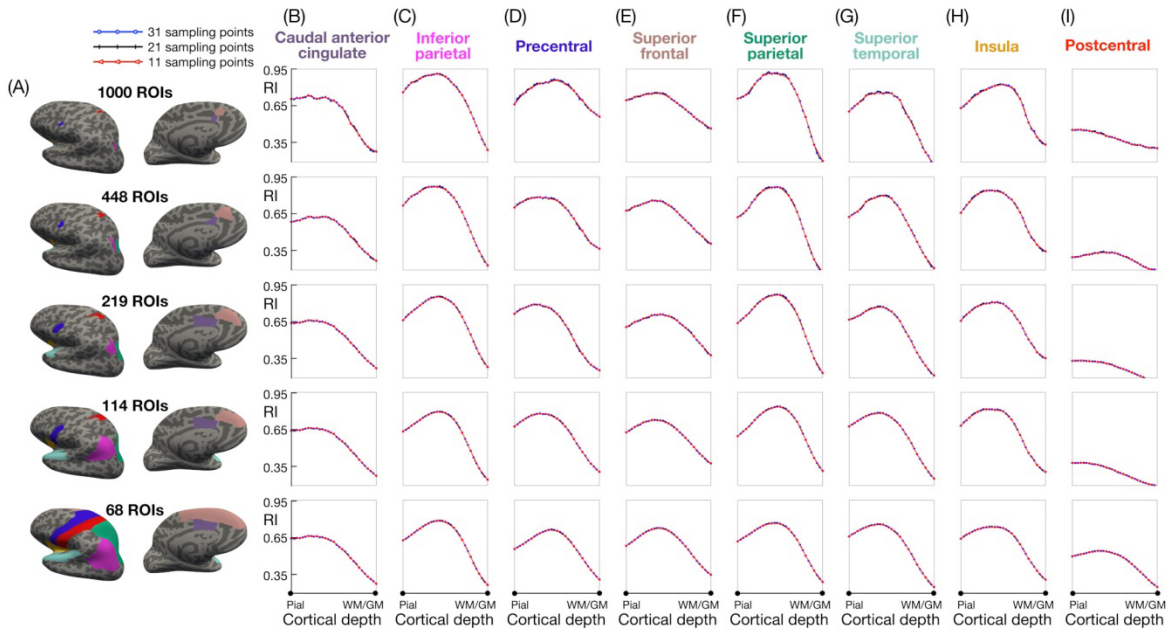

Supplementary Figure S11: (**A**) 8 representative ROIs from each of the 5 atlases. (**B-I**) RI vs. cortical depth profiles in each of these ROIs from subject 3 obtained with 11, 21, or 31 sampling points (i.e., with a step size of 10%, 5%, and 3.33% of the cortical thickness, respectively) (and with all other parameters in the data analysis pipeline as used in Fig. 4).

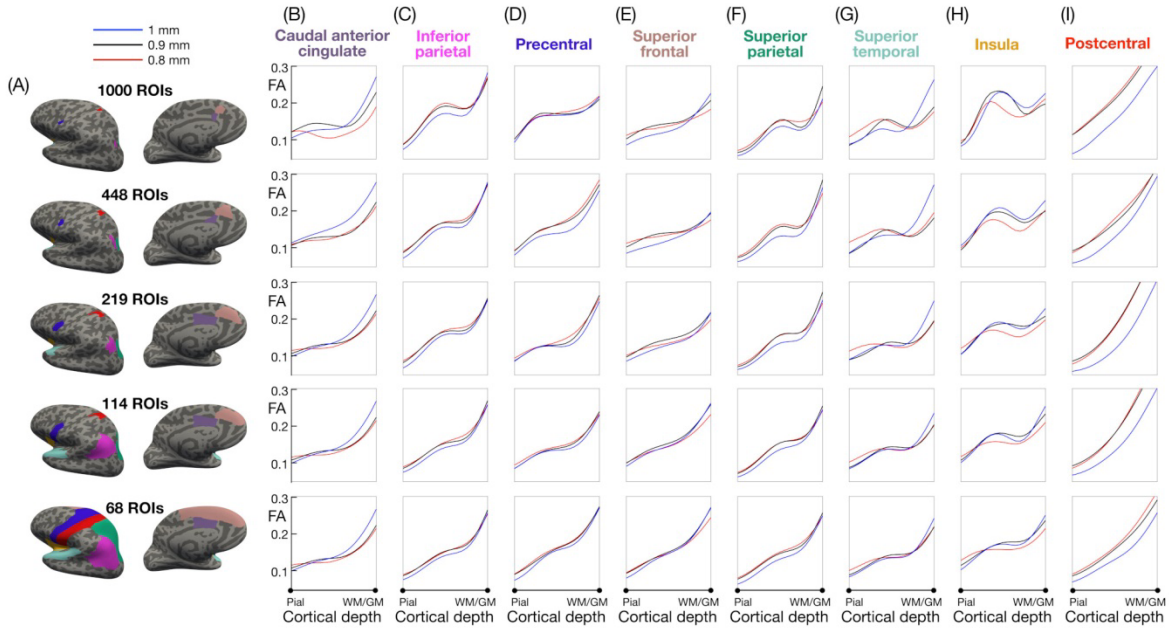

Supplementary Figure S12: (**A**) 8 representative ROIs from each of the 5 atlases. (**B-I**) FA vs. cortical depth profiles in each of these ROIs from subject 3 obtained with a spatial resolution of 0.8, 0.9, or 1.0 mm isotropic for both the DTI and anatomical scans (and with all parameters in the data analysis pipeline as used in Fig. 4).

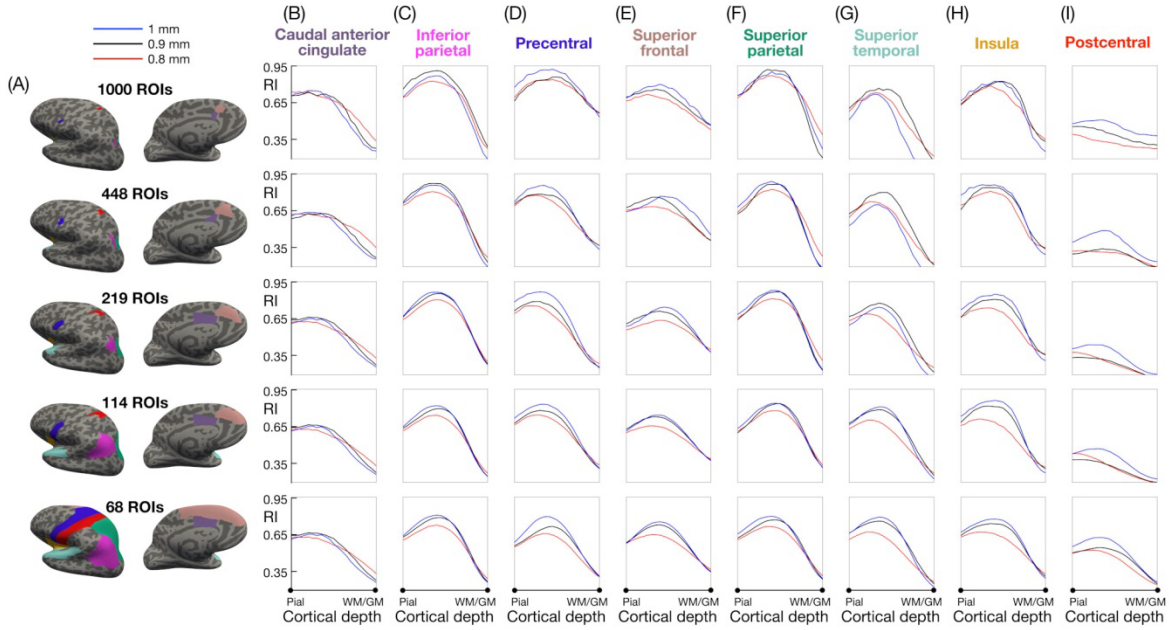

Supplementary Figure S13: (**A**) 8 representative ROIs from each of the 5 atlases. (**B-I**) RI vs. cortical depth profiles in each of these ROIs from subject 3 obtained with a spatial resolution of 0.8, 0.9, or 1.0 mm isotropic for both the DTI and anatomical scans (and with all parameters in the data analysis pipeline as used in Fig. 4).

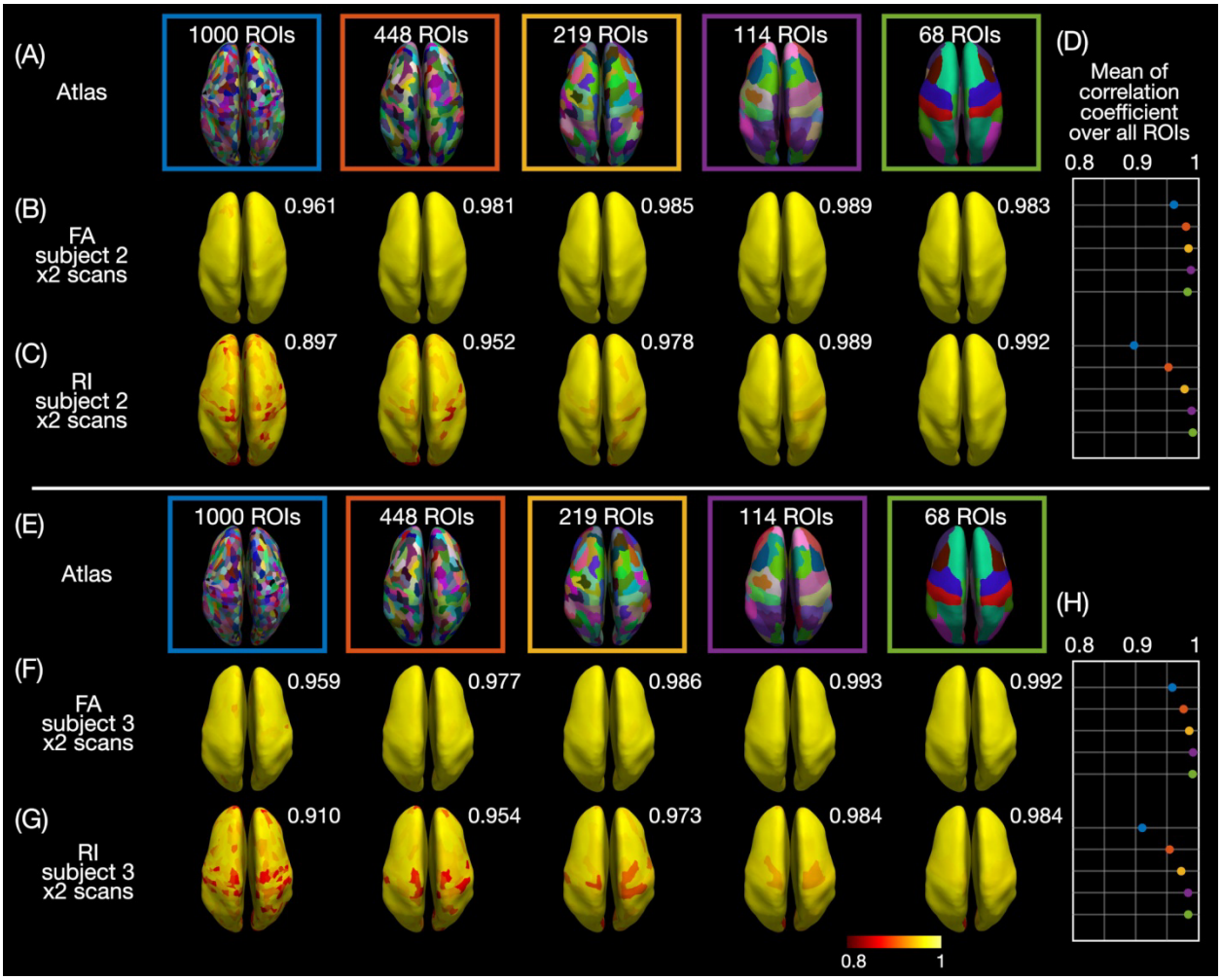

Supplementary Figure S14: (**A,E**) ROIs from the 5 atlases displayed on the inflated cortical surfaces of subjects 2 and 3. Correlation coefficient of the FA (**B,F**) or RI (**C,G**) vs. cortical depth profiles between both DTI scans of subjects 2 and 3 calculated in

each ROI and displayed on inflated cortical surfaces. (**D,H**) Plot of the mean correlation coefficients averaged over all ROIs (also shown at the top right corner of each brain).

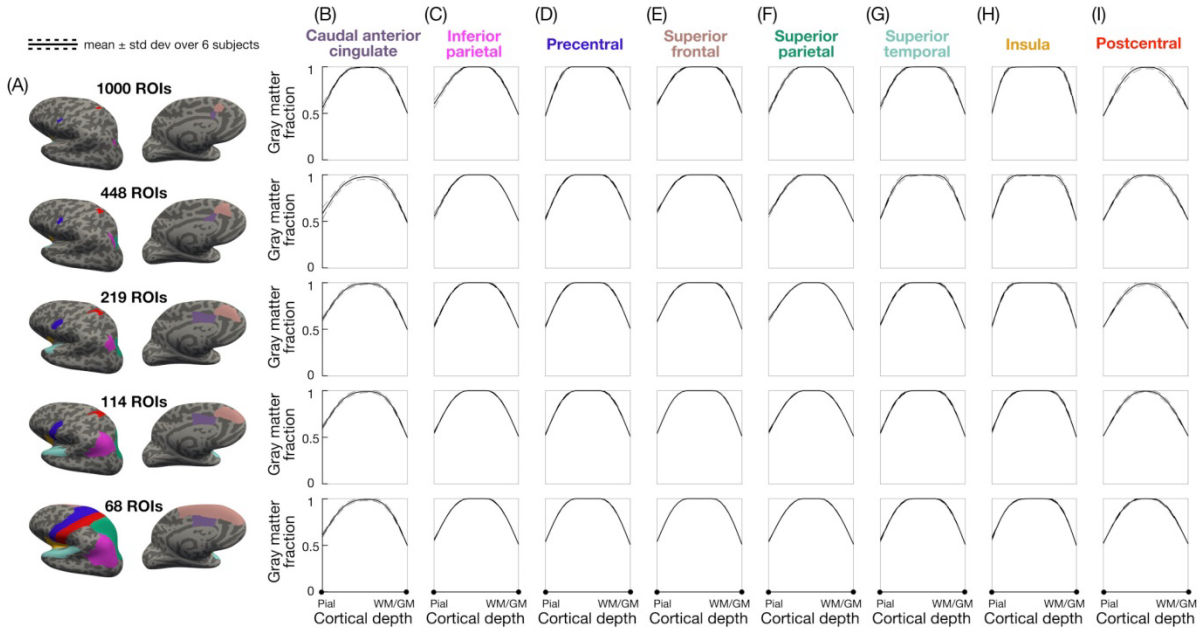

Supplementary Figure S15: (**A**) 8 representative ROIs from each of the 5 atlases. (**B-I**) Mean (solid lines) ± standard deviation (dashed lines) across the 6 subjects of the GM fraction vs. cortical depth profiles in each of these ROIs.

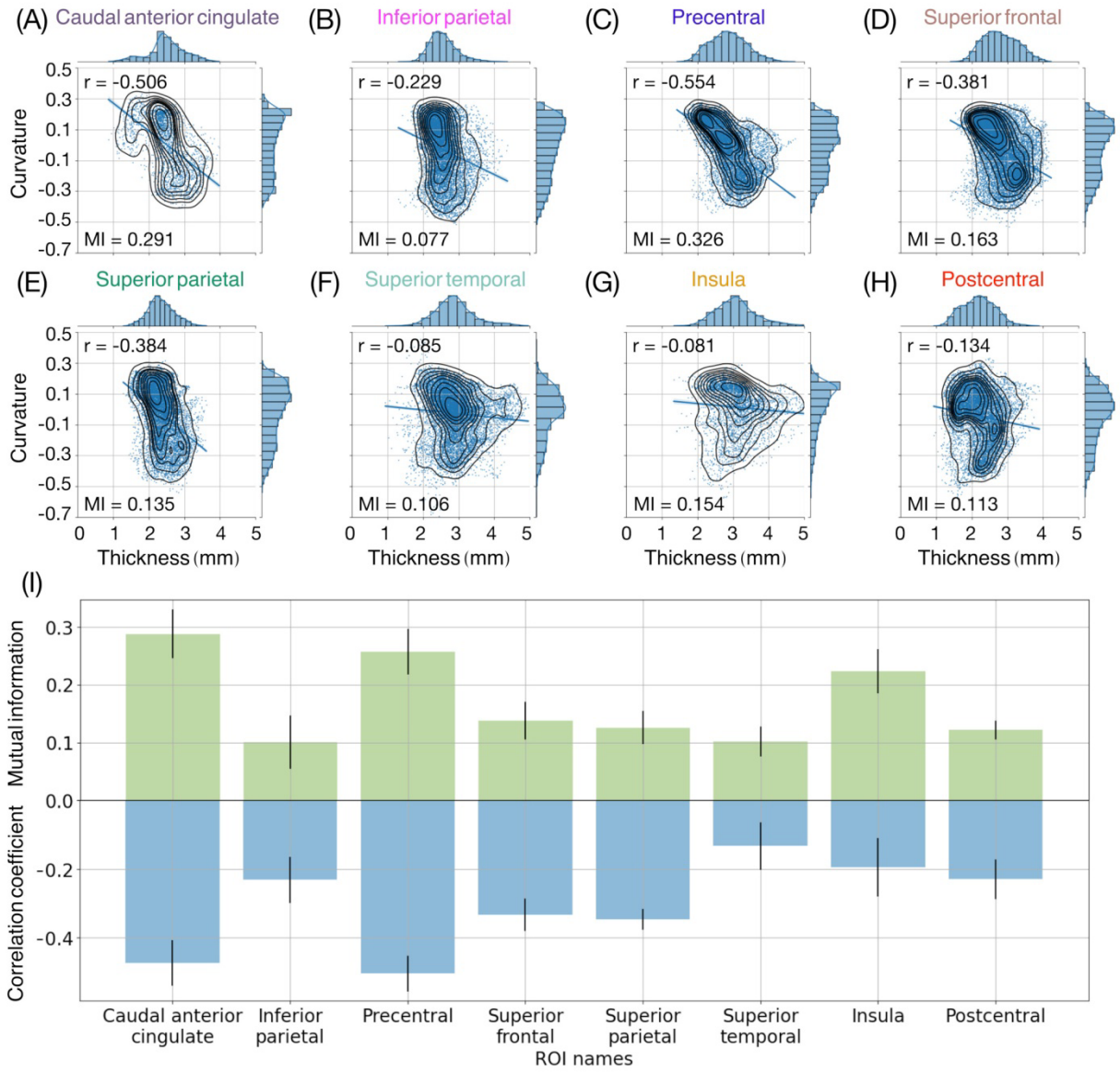

Supplementary Figure S16: (A–H) Scatter plots of the cortical curvature vs. cortical thickness in 8 representative ROIs from subject 3 (from the atlas with 68 ROIs), along with the corresponding linear regression (blue line), kernel density estimation (black lines), histograms, Pearson's correlation coefficient (r), and mutual information (MI). (I) Mean ± standard deviation across all subjects of the correlation coefficient and mutual information.